Local suppression of the hidden-order phase by impurities in URu_{2}Si_{2}

Maria E. Pezzoli, Matthias J. Graf, Kristjan Haule, Gabriel Kotliar, and Alexander V. Balatsky

Phys. Rev. B **83**, 235106 — Published 6 June 2011

DOI: 10.1103/PhysRevB.83.235106

Local suppression of the hidden order phase by impurities in URu_2Si_2

Maria E. Pezzoli,[1] Matthias J. Graf,[2], Kristjan Haule[1], Gabriel Kotliar[1] and Alexander V. Balatsky [2,3]
[1] *Serin Physics Laboratory, Rutgers University, Piscataway, NJ 08854, USA.*
[2] *Theoretical Division, Los Alamos National Laboratory, Los Alamos, NM 87545, USA.*
[3] *Center for Integrated Nanotechnology, Los Alamos National Laboratory, Los Alamos, NM 87545, USA.*

We consider the effects of impurities on the enigmatic hidden order (HO) state of the heavy-fermion material URu_2Si_2. In particular, we focus on local effects of Rh impurities as a tool to probe the suppression of the HO state. To study local properties we introduce a lattice free energy, where the *time invariant* HO order parameter ψ and local antiferromagnetic (AFM) order parameter M are *competing orders*. Near each Rh atom the HO order parameter is suppressed, creating a hole in which local AFM order emerges as a result of competition. These local holes are created in the fabric of the HO state like in a Swiss cheese and "filled" with droplets of AFM order. We compare our analysis with recent NMR results on $U(Rh_xRu_{1-x})_2Si_2$ and find good agreement with the data.

PACS numbers: 71.27+a, 75.40.Mg, 76.60.-k, 74.62.Dh

I. INTRODUCTION

The physics of heavy-fermion materials is fascinating and extremely challenging due to a variety of exotic phenomena that can be observed, *e.g.*, the Kondo effect, the heavy mass renormalization, the onset of novel magnetism or of unconventional superconductivity. The interplay between these phenomena makes a detailed understanding of the ground state complicated. Here we focus on URu_2Si_2, the heavy-fermion material that exhibits a "hidden order" (HO) phase below $T_{\rm ho} = 17.7$K[1]. The specific heat of this material displays the typical jump of a second order phase transition at $T_{\rm ho}$, however the precise nature of the HO remains a subject of intensive debate. Far above the HO transition the magnetic susceptibility has a maximum around $T \sim 50$K[1]. The measured magnetic moment reported by neutron scattering, if there is any, is too small ($\sim 0.03\,\mu_B/U$) to explain the large entropy loss at $T_{\rm ho}$ within a localized AFM scenario, which led to the concept of the small moment antiferromagnetism[2]. Early μSR (muon spin relaxation) measurements reported magnetic moments as small as $\sim 10^{-3}\,\mu_B/U$[3]. However, later μSR and nuclear magnetic resonance (NMR) measurements on pure URu_2Si_2 revealed an inhomogeneous coexistence between the HO and AFM order with a sizable magnetic moment[4,5]. Moreover recent neutron scattering experiments evidence that this small moment is not an intrinsic feature of the HO, but a spurious effect due to local strains induced by crystal defects in the sample[6]. Nevertheless magnetic ordering is not completely extraneous to URu_2Si_2: an antiferromagnetic phase with large moment can be stabilized by applying pressure or strain[5,7–9]. Since 1985 several theories have been proposed to identify the nature of the hidden order parameter. Recently a resurgence of interest in this material has been seen as new data and new ideas on the nature of the HO appeared[10–17].

Further progress in experimental techniques such as sample quality and more accurate measurements of URu_2Si_2 suggest that a breakthrough in this long standing problem is at hand and may be achieved soon. In this paper we focus on the role of impurities as probes of the nature of the hidden order puzzle. We address the role of deliberately placed Rh impurities on the suppression of the HO state. Since few impurities are added to the sample, NMR is a particularly useful bulk probe sensitive to the local atomic environment to reveal what happens to the HO state at the impurity site. Recently the ^{29}Si NMR spectrum has been reported in $U(Ru_{1-x}Rh_x)_2Si_2$ as a function of temperature and Rh concentration[18]. The experiment showed local suppression of the HO state and the emergence of satellite NMR peaks, indicating the onset of *local* antiferromagnetic droplets near each Rh impurity. These experiments were interpreted in a Ginzburg-Landau framework, where antiferromagnetism and hidden order are coupled through gradient terms. In this scenario the antiferromagnetism is not a competing order parameter but rather a parasitic effect induced by spatial inhomogeneities in the hidden order parameter[18].

Here we turn to a more microscopic description of the effects of impurities at the atomic length scale by using a *lattice free energy*, where each lattice site corresponds to a uranium atom. We thus extend earlier work, using a lattice free energy with parameters describing the phase diagram of URu_2Si_2[19] in presence of pressure and strain, in order to address a spatially inhomogeneous setting. The approach is not tied however to a specific microscopic origin of the hidden order: the form of the lattice free energy is general and we choose a particular set of parameters values since it has been proven to be consistent with experiment. In this model droplets emerge around the impurities as a result of the competition between the HO and AFM order, enhanced by the coupling mechanism suggested in Ref. 18.

The paper is organized as follows: in Sec. II we introduce the lattice free energy that we minimize in order to determine the phase diagram of $U(Ru_{1-x}Rh_x)_2Si_2$; in Sec. III we show our results and compare them with recent experimental NMR data[18]; in Sec. IV we draw our conclusions. Finally in appendix A we discuss how

the lattice free energy can be derived from a microscopic Hamiltonian and in appendix B we derive the coarse-grained Ginzburg-Landau free energy from our lattice free energy model to make contact with earlier work[18].

II. MODEL

We write the free energy in terms of two order parameters: the HO parameter ψ_i and the AFM order parameter M_i. M_i is the z component of the magnetic moment, since it is observed experimentally that URu_2Si_2 orders magnetically along the z direction[2,5,20]. The free energy contains three terms: $F = F_\psi + F_M + F_c$, where F_c is the coupling term between ψ_i and M_i . Assuming that the hidden order preserves time-reversal symmetry, the simplest form of F_c is $F_c = g_1 \sum_i \psi_i^2 M_i^2$ [21]. Therefore we can write the lattice free energy as

$$\begin{aligned} F = & a_\psi \sum_i \psi_i^2 + b_\psi \sum_i \psi_i^4 + \frac{1}{2}\sum_{ij} J_{ij}^\psi \psi_i \psi_j \\ & + a_M \sum_i M_i^2 + b_M \sum_i M_i^4 + \frac{1}{2}\sum_{ij} J_{ij}^M M_i M_j \\ & + g_1 \sum_i \psi_i^2 M_i^2 \ , \end{aligned} \quad (1)$$

where ψ_i and M_i are defined for each site of a three dimensional lattice.

The form of this lattice free energy is general and can accommodate different scenarios for the hidden order in URu_2Si_2. As discussed in the appendices, the information about the underlying microscopic theory is contained in the values of the lattice free energy parameters. A similar phenomenological free energy was proposed for a toy model describing the competing AFM and hexadecapolar order emerging from crystal field splitting within the unit cell of URu_2Si_2[19]. In that case, the parameters were naturally expressed in terms of an effective crystal field splitting Δ at each uranium site: $a_\psi = a_M = a = \frac{\Delta}{2}\coth(\frac{\Delta}{2T})$, $b_\psi = b_M = b = \frac{\Delta}{2}[\sinh(\frac{\Delta}{T}) - \frac{\Delta}{T}]\frac{\cosh^2(\Delta/2T)}{\sinh^4(\Delta/2T)}$ and $g_1 = 2b$. The effective exchange constants J^ψ and J^M were determined in such a way to reproduce the experimentally observed critical temperatures, *i.e.*, the hidden order transition temperature at zero doping $T_{\rm ho} = 17.7$K and the Neel temperature $T_{\rm N} = 15.7$K, that is $J^\psi = \Delta/\tanh(\Delta/2T_{\rm ho})$ and $J^M = \Delta/\tanh(\Delta/2T_N)$[22]. This parametrization of the lattice free energy, using the measured elastic constants, was shown to provide an excellent description of the phase diagram of URu_2Si_2 under applied magnetic field, pressure and strain . Here $\Delta = 35$K is the effective crystal field splitting between the two lowest lying states of the U atom $5f$ electrons of URu_2Si_2 in the paramagnetic phase[15]. In this work we choose to adopt the same parametrization. We stress however that the form of this free energy is much more general and describes a situation where ψ_i is any order parameter that does not break time-reversal symmetry; for example, alternative time invariant order parameters are a charge density wave at *incommensurate* momenta[12], a hybridization wave[23,24] or quadrupolar order[25–27]. Hence spin density wave[28], octupolar and triakontadipolar[29] order are not included, since they change sign under time reversal.

To incorporate the role of impurities we consider two effects. The first is a mean-field effect in which we regard the coefficients a and b to be disorder dependent. In an itinerant picture the presence of disorder creates a random potential acting on the electrons: the impurities act as scattering centers which reduce the excitonic pairing in the particle hole channel. In the model of Ref. 19, the impurity induced strain increases the crystal field parameter Δ and therefore it suppresses both the antiferromagnetism and the hidden order stabilizing the paramagnetic phase. The coefficients a and b thus acquire a linear (at leading order) dependence on doping x by imposing $\Delta(x) = \Delta_0 + x\Delta_1$. However we keep the definition of J^ψ and J^M to be disorder independent, *i.e.* $J^\psi = \Delta_0/\tanh(\Delta_0/2T_{\rm ho})$ and $J^M = \Delta_0/\tanh(\Delta_0/2T_N)$. With this parametrization

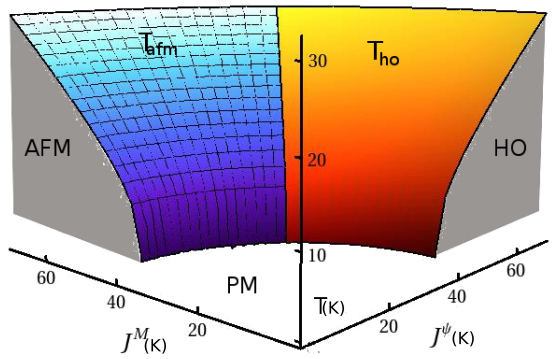

FIG. 1. (Color online) Phase diagram of the lattice free energy described in the text in the J^ψ, J^M, T space at doping $x = 0$.

there is a duality between hidden order ψ and large antiferromagnetic moment M. When $J^\psi > J^M$ the hidden order phase is stabilized at low temperature; if $J^M > J^\psi$ the large moment phase is stabilized. In Fig. 1 we show the phase diagram of the homogeneous lattice free energy of Eq. 1 with the choice of parameters discussed above, in the (J^ψ, J^M, T) parameter space. The introduction of impurities, through the disorder dependence of the mean-field coefficients a and b, suppresses equally both HO and AFM order parameters.

Doping URu_2Si_2 with Rh atoms has also the effect of a chemical pressure. Indeed close to Rh impurities HO is suppressed and local strains induce a finite moment. In our model this is explicitly described by a locally renormalized exchange term in the hole of the Swiss cheese fabric:

$$F_{\mathrm{r}_i} = -\frac{1}{2}[J^M - \tilde{J}^M] \sum_{\vec{d}=\pm 1} M_{\mathrm{r}_i} M_{\mathrm{r}_i+\vec{d}} \quad (2)$$

where $\tilde{J}^M > J^\psi$ and by imposing $\psi(r_i) = 0$. As a result, away from the impurities $J^M < J^\psi$ and the hidden order is stable, but in the immediate vicinity of the impurity antiferromagnetism is stabilized over hidden order. In order to study the local suppression of the hidden order by impurities, we consider the lattice model described by the free energy

$$F_{\rm impurities} = F + \sum_i F_{{\rm r}_i} \, . \tag{3}$$

To introduce a minimum number of parameters we limit the range of the interaction to only the first neighbors of the affected uranium site. Given these definitions, the free parameters of the model are the magnetic coupling $\tilde{J}^M$ at the impurity sites and Δ_1. Due to the duality of the model, as magnetic droplets can be stabilized in a hidden order background, with the same mechanism droplets of "hidden order" could be stabilized within the large moment phase by another type of impurity, which would exchange the role of J^M and $\tilde{J}^M$. It would be interesting to see if it is possible to realize this dual scenario experimentally. The existence of localized regions of the HO phase in the AFM phase at higher pressure could be observed in NMR experiments and other local probes. The counterpart of the previous $URu_{1-x}Rh_xSi_2$ experiment would require to measure URu_2Si_2 under pressure to stabilize AFM but doped with suitable impurities to induce a local expansion in the ab plane. In the numerical simulations we assume that the disorder is dilute enough to consider the local solution around a single impurity at r_0 in the background of uniform disorder. Hence, we assume a mean-field approximation for doping-renormalized coefficients $a(x)$ and $b(x)$ through their dependence on the crystal field parameter $\Delta(x)$. For simplicity, we neglect any mean-field doping effects on the effective exchange constants J^ψ and J^M, however, we explicitly account for the spatial variation of J^M through $\tilde{J}^M$ in the immediate vicinity of the impurity (see Eq. 3) In this work we take a simplified cubic lattice instead of the tetragonal lattice of URu_2Si_2, and we do not consider the problem of how the order parameter on the U atoms is transferred to the nuclear sites of the Si where the NMR is performed. Our goal in this paper is to explore the physics introduced by inhomogeneities using a lattice free energy framework and see how the NMR experiments constrain the symmetry and the parameters in this theory. We test whether the parametrization of the lattice free energy that was used to successfully describe the phase diagram of URu_2Si_2 under pressure, stress and applied magnetic field can also account qualitatively for the puzzling NMR measurements when impurities are introduced in the sample.

Once we define the lattice free energy, we determine the value of ψ_i and M_i that minimize the free energy, *i.e.* the solutions to the equations

$$\begin{aligned} \frac{\delta F_{\rm impurities}}{\delta \psi_i} &= 0 \\ \frac{\delta F_{\rm impurities}}{\delta M_i} &= 0 \, . \end{aligned} \tag{4}$$

Notice that, away from the impurity, the solutions are $M_i^2 = 0$ and $\psi_i^2 = \frac{J^\psi - 2a(T,x)}{4b}$ for each site i (at large enough distance from the impurity the lattice translational invariance is restored).

III. RESULTS

We first compute the HO critical temperature as a function of doping x. Since we assume dilute doping, the hidden order critical temperature $T_{\rm ho}(x)$ is very well approximated by

$$T_{\rm ho}(x) = \frac{\Delta_0 + x\Delta_1}{2\,{\rm artanh}(\frac{\Delta_0 + x\Delta_1}{J^\psi})} \, . \tag{5}$$

At the critical doping x_c the HO parameter vanishes and $T_{\rm ho}(x_c) = 0$; it follows that x_c is given by $\Delta_0 + x_c\Delta_1 = J^\psi$. In Fig. 2 we compare the theoretical curve (5)

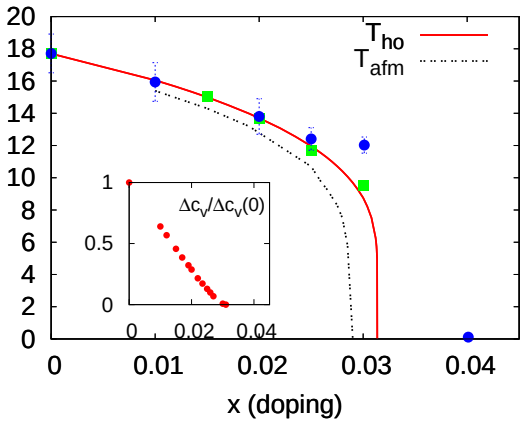

FIG. 2. (Color online) Computed critical temperature $T_{\rm ho}$ for the order parameter ψ as a function of doping. Squares and circles are experimental values taken respectively from Ref. 18 and Ref. 30. The dashed line corresponds to the temperature $T_{\rm afm}$ at which the magnetic signal disappears according to our calculation. Inset: computed jump of the specific heat $\Delta c_v/\Delta c_v(0)$ at the phase transition as a function of doping. $\Delta c_v(0)$ is the value of the jump at zero doping.

for $\Delta_1 = 358.6$K with experimental data[18,30]. J^ψ and Δ_0 have been defined above for the uniform case and are equal to $J^\psi = 46.24$K and $\Delta_0 = 35$K. We observe that the transition temperature, up to leading terms, has in our model the usual linear dependence on x similar to impurity-averaged theories. In the inset of Fig. 2 we report the computed jump in the specific heat

$\Delta c_v = \frac{-1}{V}\frac{\partial^2 F}{\partial T^2}$. Since the free parameter Δ_1 was determined by the critical temperature the agreement with the experimental data is very satisfactory[18]. In Fig. 2 we plot also T_{afm} as a function of doping. T_{afm} is defined as the temperature at which the magnetization becomes smaller than the minimum observed magnetic moment $\mu_{0,\min} \approx 0.03\ \mu_B$.

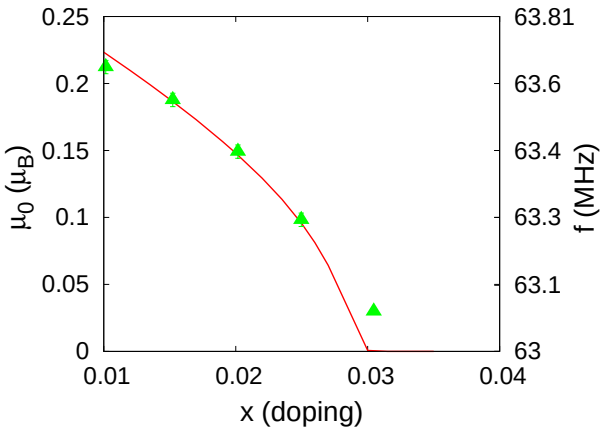

FIG. 3. (Color online) Magnetic moment induced by the Rh impurities, in units of μ_B (left axis) and in units of the corresponding NMR frequency (right axis) as a function of x at $T = 4$ K. The frequencies of the two satellite peaks are $f_\pm = \gamma(H_0 \pm A\mu_0)(1+K)$, where $\gamma = 8.46\,\mathrm{MHz/T}$ is the gyromagnetic ratio of ^{29}Si, $K = 0.065$ is the Knight shift, $H_0 = 7\,\mathrm{T}$ is the external field, $A = 0.36\,\mathrm{T}/\mu_B$ is the hyperfine coupling and μ_0 is the ordered spin moment of U atoms. The red line is the result of our model, while full triangles are experimental points taken from Ref. 18. The computed magnetic moment is the value of the magnetization at the impurity site.

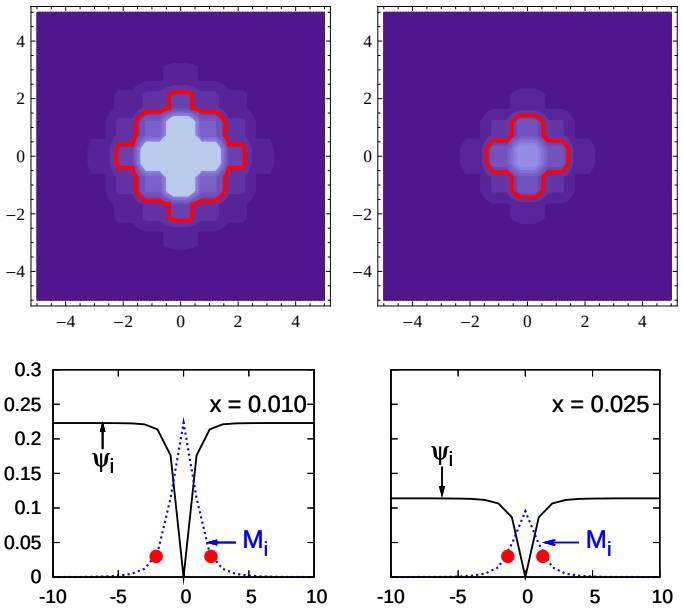

FIG. 4. (Color online) Upper panels: magnetization density in the plane $z = 0$ at $T = 4$K for Rh concentration $x = 0.01$ (left) and $x = 0.025$ (right). We display the magnetization in the interval $[0.002, 0.22]$: brighter colors correspond to higher values. The red contour corresponds to the magnetic droplet boundary as defined in the text. Lower panels: profile of the magnetization M_i (blue dashed line) and of the HO order parameter ψ_i (black solid line) along the direction (0,y,0) of the lattice. Red dots correspond to the intersection of the magnetization with droplet boundaries.

In Fig. 3 we report the NMR frequencies f as a function of Rh concentration x. The NMR frequency f is proportional to the spin moment μ_0 at each U site, in particular $f_\pm = \gamma(H_0 \pm A\mu_0)(1+K)$, where $\gamma = 8.46\,\mathrm{MHz/T}$ is the gyromagnetic ratio of ^{29}Si, $K = 0.065$ is the Knight shift, $H_0 = 7\,\mathrm{T}$ is the external field, $A = 0.36\,\mathrm{T}/\mu_B$ is the hyperfine coupling. In our model we identify the magnetization at the impurity site M_{r_0} with μ_0. The theoretical curve in Fig. 3 is obtained with $\tilde{J}^M = 52.64$K.

From the NMR spectrum we obtain another valuable information: the area under the satellite peaks is proportional to the fraction of antiferromagnetic sites, *i.e.* the ratio between sites with a finite magnetization and the total number of sites. The measured antiferromagnetic fraction has a non-monotonic behavior as a function of the Rh concentration x: first it increases linearly with the number of impurities, then it reaches a maximum at $x = 0.025$ and finally it decreases becoming zero after the critical concentration has been reached[18]. Our model offers a simple explanation of this non-monotonic behavior. In Fig. 4 a real-space representation of the magnetization M_i at each site is reported for impurity concentrations $x = 0.01$ and $x = 0.025$. The sites around the impurity develop a finite moment. The moment at each site decreases as the distance from the impurity increases. The magnetization is strongly suppressed and ψ_i recovers the bulk solution value within few lattice sites, see profile picture in Fig. 4. In the following we will refer to the magnetic sites around the impurity with the term "droplet". We define the droplet boundary in such a way that the magnetization of every site inside the droplet is large enough to be observed experimentally. We consider that the minimum observed magnetic moment is equal to $\mu_{0,\min} = 0.03\ \mu_B$. We can see in Fig. 4 that the size of the droplet is affected by disorder. The two competing effects of disorder are evident: on the one hand the number of magnetic droplets increases with the number of impurities, on the other hand in our model the size of each droplet decreases with increasing disorder. This leads to the observed non-monotonicity in the experiments. Notice that, in a model where HO and AFM order are coupled through a term $M^2|\vec{\nabla}\psi|^2$, the behavior of magnetic droplets in function of doping is similar[18].

In order to put this analysis on more quantitative grounds, we optimize the free energy for different values of temperature and Rh concentration and then we compute the fraction of sites with $M_i \neq 0$ ($M_i > \mu_{0,\min}$).

Since we made the assumption that magnetic droplets are disjoint with average spacing $d \sim l/x^{1/3} > 1$ nm (here l is the lattice constant), we can define the antiferromagnetic fraction in the following way

$$\text{AFM fraction} = \frac{n_{\text{in}} \times n_{\text{imp}}}{N_{\text{tot}}} = n_{\text{in}} \times x \ , \qquad (6)$$

where n_{in} is the number of sites inside the droplet, n_{imp} is the number of impurities and N_{tot} is the total number of sites. In figure 5, upper panel, we plot the AFM fraction

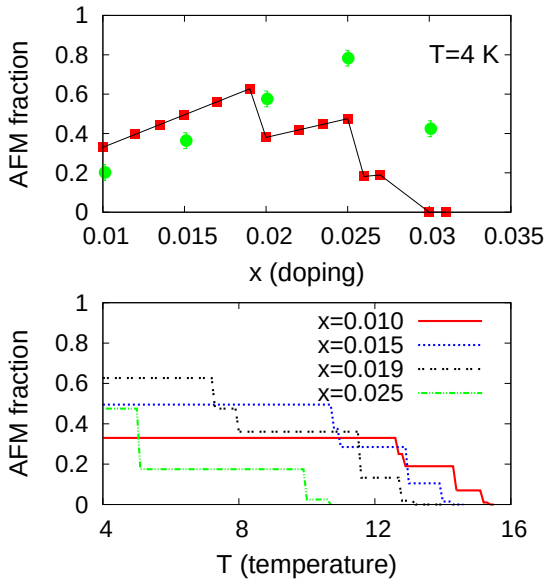

FIG. 5. (Color online) Upper panel: comparison between the measured (green circles) and the computed (red squares) AFM fraction, as defined in the text, for different values of Rh concentration at temperature $T = 4$K. The black line is a guide to the eye. Lower panel: computed AFM fraction as a function of temperature T for different values of the Rh concentration x.

as a function of doping. The curve has the characteristic non-monotonic behavior of the experimentally observed AFM fraction, which highlights the two competing effects of disorder: the chemical pressure and the suppression of order. Crucial to this observation is the duality between ψ and M, and hence the fact that Rh impurities suppress both order parameters. While the sawtooth profile is a consequence of our lattice model, there is good agreement between the results of the minimization procedure and experiment. The sawtooth profile appears because the number of sites with $M_i > \mu_{0,\text{min}}$ is a step function of x. In fact lowering the temperature below T_N the first site to be magnetized is the impurity site r_0, then the nearest neighboring sites, followed by the next-nearest neighbors and so on. Therefore the droplet size increases (and with the same mechanism the droplet decreases as a function of doping) in steps equal to the coordination number. In the lower panel of figure 5 we plot the AFM fraction as a function of temperature. At low temperature the AFM fraction is a non-monotonic function of x as discussed above; increasing the temperature the magnetic droplet can be stabilized only for lower doping values. We identify with T_{afm} the temperature in correspondence to the disappearance of the magnetic droplet for a given Rh concentration. We observe that at large doping T_{afm} follows the behavior of T_{ho} as a function of x, see Fig. 2.

The emergence of a magnetic moment in URu_2Si_2 doped with Rh has been observed also in neutron scattering experiments[30]. First, notice that the NMR and the neutron experiments are not completely compatible. For example the moment inferred from neutron scattering at $x = 0.03$ is $\sim 0.16\mu_B$ while the moment inferred from NMR at the same nominal concentration is $\sim 0.03\mu_B$. Also neutrons suggest that the effect of Rh atoms is different in the low doping ($x < 0.01$) and high doping regime ($x > 0.01$), while in the NMR experiment there is no dramatic difference between the two doping regimes. Nevertheless, we can qualitatively interpret these experiments if we envision AF droplets which are very anisotropic and concentrated at stacking faults along the c axis as suggested in Ref. 20; that even at $x = 0$ there are some defects present which can nucleate some AF regions. The presence of defects is required to explain the $x = 0$ experiment as stressed earlier in the pioneering work by Amitsuka[31]. The anisotropy of the droplets is required to account for the long correlation length in the ab plane observed by neutrons[30]. The abrupt change from $x = 0.01$ to $x = 0.02$ observed by neutrons could be due to the crossing of a percolation threshold of the AF droplets. We stress that at this point the calculations were based on a very simplified model and further progress in the interpretation of neutrons and NMR experiments would require the modeling of the hyperfine fields, the realistic determination of the structure of the droplet and the calculation of the neutron magnetic structure factor. This is indeed a very interesting subject, which however goes beyond the scope of the present work. In this work we have chosen to explain the basics physics of URu_2Si_2 doped with Rh as it emerges from the reported NMR experiment; indeed the free energy lattice model here studied succeeds in reproducing many basic features of the NMR result.

IV. CONCLUSION

In conclusion, we proposed an analysis within a mean-field lattice free energy to reveal the local competition between HO and AFM phase. We introduced disorder in the model as the driving force of two competing effects: the local stabilization of magnetization and the suppression of both the HO and AFM order by the impurity. We recovered the main features of the phase diagram and the non-monotonic behavior of the AFM volume observed experimentally. Moreover, we found that the healing lengths of ψ_i and M_i are on the scale of the

local strains that stabilize the magnetization. An additional effect present in the calculation is the stabilization of the phases due to inhomogeneities pointed out in Ref. 18, which is manifest in the continuum theory supported by our lattice model as shown in Appendix B. Finally our model describes a duality between HO and AFM order: as magnetic droplets can be stabilized by impurities in the HO phase, with a similar mechanism HO droplets can be formed in a magnetic phase.

We used in this paper a classical lattice free energy. Since the phase transitions occur at rather low temperatures, it would be interesting to extend our work to include quantum effects, including effects which would be described by time derivatives of the order parameter as well as the effects of damping due to particle-hole excitations. The study of these effects as well as their derivation from microscopic models will provide further constraints on the possible origin of the hidden order state in URu_2Si_2. This would allow also a more refined modeling of the NMR line-shapes and the mechanism for the transfer of the hyperfine fields from the uranium to the ligand site.

Acknowledgments: We are grateful to N. Curro, S. H. Baek, J.C. Davis, and Marcel Porta for useful discussions. This work was supported by US DOE, under BES and UCOP010 funding. GK and MP acknowledge the support of DOE BES DE-FG02-99ER45761 and subcontract 83509-001-10 to Rutgers. KH was supported by the ACS Petroleoum Research Fund 48802 and Alfred P. Sloan foundation.

Appendix A: Mapping from microscopic Hamiltonian onto the lattice free energy

A general and formal expression for the lattice free energy in terms of the HO and AFM order parameters ψ_i and M_i is given by

$$\begin{aligned} Z &= \int \mathrm{d}\lambda_1 \int \mathrm{d}\lambda_2 \int \mathcal{D}\Psi \mathcal{D}\Psi^\dagger e^{-\int \mathrm{d}x \mathcal{L}[\Psi^\dagger,\Psi] + \sum_i \lambda_{1,i}\left(O_1([\Psi^\dagger\Psi]_i) - \psi_i\right) + \sum_i \lambda_{2,i}\left(O_2([\Psi^\dagger\Psi_i]) - M_i\right)} \\ &= e^{-\beta F[\psi_i, M_i]} \end{aligned} \tag{A1}$$

The Lagrangian $\mathcal{L}[\Psi^\dagger, \Psi]$ is the starting point of the calculation written in terms of creation and annihilation operators containing all the relevant bands. The starting point can be simplified depending on the itinerant or localized model one considers and on the full quantum many-body Hamiltonian. However, in the general case the evaluation of the free energy is more involved and will not be attempted here. ψ and M are two order parameters with ψ time reversal invariant and M breaking time reversal symmetry, the index i runs over the lattice positions of the U atoms. Different proposals of the hidden order differ in the definition of the operator O_1. In the proposal of Ref. 12 the hidden order is a charge density wave with incommensurate wave vector $\vec{Q}^*$, and in this case the condensate is related to the Fourier transform of $O_1([\Psi^\dagger\Psi]_i)$

$$O_1([\Psi^\dagger\Psi]) = \sum_{\vec{k},\sigma\sigma'} \Psi^\dagger_\sigma(\vec{k} - \vec{Q}^*)\Psi_{\sigma'}(\vec{k})_{\sigma'}\delta_{\sigma,\sigma'}\,. \tag{A2}$$

For a hexadecapolar order as in Ref. 19 the operator O_1 is equal to

$$O_1([\Psi^\dagger\Psi]) = C\sum_{kk'}\sum_{\sigma\sigma'} F_{\sigma\sigma'}(\vec{k},\vec{k}')\Psi^\dagger_\sigma(\vec{k} - \vec{Q})\Psi_{\sigma'}(\vec{k}') \tag{A3}$$

where C is a normalization constant, $\vec{Q}$ is the commensurate ordering vector and $F_{\sigma\sigma'}(\vec{k},\vec{k}')$ are defined by

$$\begin{aligned} F_{\uparrow\downarrow}(\vec{k},\vec{k}') &= \frac{3\sqrt{5}}{64\pi}\left[5\sqrt{7}(k_x - ik_y)^3(k'2_x - ik'_xk'_y - k'^2_y)k'_z - (k_x^2 + ik_xk_y - k_y^2)k_z(ik'_y + k'_x)(-1 + 5k'^2_z)\right]\gamma_k\gamma^*_{k'} \\ F_{\downarrow\uparrow}(\vec{k},\vec{k}') &= \frac{3\sqrt{5}}{64\pi}\left[5\sqrt{7}(k_x + ik_y)^3(k'^2_x + ik'_xk'_y - k'^2_y)k'_z - (k_x^2 - ik_xk_y - k_y^2)k_z(k'_x - ik'y)(-1 + 5k'^2_z)\right]\gamma_k\gamma^*_{k'} \\ F_{\uparrow\uparrow}(\vec{k},\vec{k}') &= \frac{3\sqrt{5}}{64\pi}\left[5(k_x^2 - ik_xk_y - k_y^2)k_z(k'^2_x - ik'_xk'_y - k'^2_y)k'_z - (k_x - ik_y)^3(k'_x - ik'_y)(-1 + 5k'^2_z)\right]\gamma_k\gamma^*_{k'} \\ F_{\downarrow\downarrow}(\vec{k},\vec{k}') &= \frac{3\sqrt{5}}{64\pi}\left[5(k_x^2 + ik_xk_y - k_y^2)k_z(k'^2_x + ik'_xk'_y - k'^2_y)k'_z - (k_x + ik_y)^3(k'_x + ik'_y)(-1 + 5k'^2_z)\right]\gamma_k\gamma^*_{k'}\,, \end{aligned} \tag{A4}$$

with $\gamma_k = 4\pi\int \mathrm{d}r\; r^2 j_3(kr)R(r)$. In the definition of γ_k, $R(r)$ is the radial wave function of the f-electrons and $j_3(kr)$ is the spherical Bessel function of order 3. The

operator O_2 is the magnetization operator

$$O_2([\Psi^\dagger\Psi]) = \frac{-2\mu_B}{Q^2}\sum_{\vec{k}\vec{k'},\sigma,\sigma'}\int \mathrm{d}\vec{r}e^{-i\vec{Q}\cdot\vec{r}}e^{-i\vec{k}\cdot\vec{r}}\Psi^\dagger_\sigma(\vec{k}) \times\{\vec{Q}\times\left[\frac{1}{2}\vec{\sigma}_{\sigma,\sigma'}\times\vec{Q}+\delta_{\sigma,\sigma'}\vec{\nabla}\right]e^{i\vec{k'}\cdot\vec{r}}\} \times\Psi_{\sigma'}(\vec{k'}) \tag{A5}$$

where $\vec{\sigma}$ are the Pauli matrices and $\vec{Q}$ is a reciprocal lattice vector.

From a lattice free energy perspective different *microscopic* models result in different values of the coefficients. An important coefficient is the coherence length; from the numerical simulation we estimate the coherence length for the magnetic droplet to be ~ 3 lattice constants at $T = 4$K and doping $x = 0.01$. The NMR data place important constraints on this parameter given that more itinerant models give rise to longer coherence lengths and more diffuse domain walls for the order parameter defined on the lattice scale.

Appendix B: Mapping from lattice free energies to coarse-grained Ginzburg Landau free energy

The free energy of Eq. (1) defines a model on the *lattice* describing the $5f$-U electrons in URu_2Si_2. In the continuum a Ginzburg-Landau (GL) free energy can be derived from a lattice model by suitable coarse graining. The GL description is formulated in terms of slowly varying amplitude fields $\phi(x)$. Here we describe the coarse graining starting from the microscopic free energy F used in Ref. 19. We keep higher order terms in the coupling between the hidden order parameter and the magnetization but focus only on the form of the GL action to connect it to the earlier work of Refs. 18 and 21.

The starting point is the free energy (1) on a cubic lattice introduced in Ref. 19

$$F[\psi_i,M_i,h_i^\psi,h_i^M] = \frac{1}{2}\sum_{ij}J^\psi_{i,j}\psi_i\psi_j - \sum_i h_i^\psi\psi_i + \frac{1}{2}\sum_{ij}J^M_{i,j}M_iM_j - \sum_i h_i^M M_i - \frac{1}{2}T\sum_i \log\left(\cosh\left(\frac{1}{T}\sqrt{\left(\frac{\Delta}{2}\right)^2+(h_i^\psi)^2+(h_i^M)^2}\right)\right) \tag{B1}$$

written in terms of the order parameters ψ_i, M_i and of the molecular Weiss fields h_i^ψ, h_i^M, see Ref. 19. At the extrema of the free energy h_i^ψ and ψ_i satisfy the relations $h_i^\psi = \sum_j J^\psi_{ij}\psi_j$ and $\psi_i = -\frac{h_i^\psi}{2}\tanh(\lambda_i/T\lambda_i)$ with $\lambda_i = \sqrt{(\Delta/2)^2+(h_i^\psi)^2+(h_i^M)^2}$ [19]. The same equations are satisfied by h_i^M and M_i. In Eq. (B1) we write h_i^M and h_i^ψ in terms of M_i and ψ_i exploiting the above relations and expand the free energy neglecting terms of the order of $O\left((\sum_j J^\psi_{ij}\psi_j)^2+(\sum_j J^M_{ij}M_j)^2\right)^3$ and higher. The Fourier transforms of the lattice variables ψ_i and M_i are $\psi(\vec{k}) = \frac{1}{\sqrt{N}}\sum_i e^{i\vec{k}\cdot\vec{R}_i}\psi_i$ and $M(\vec{k}) = \frac{1}{\sqrt{N}}\sum_i e^{i\vec{k}\cdot\vec{R}_i}M_i$. Since our mean-field description includes only nearest neighbors antiferromagnetic coupling, the modes that condense are $M(\vec{k}=\vec{Q})$ or $\psi(\vec{k}=\vec{Q})$ with $\vec{Q}=(\pi,\pi,\pi)$, depending on the relative size of J^ψ and J^M. The free energy of Eq. (B1) can be rewritten in terms of $\psi(\vec{k})$, $M(\vec{k})$ and the coupling constants $J^{\psi(M)}(k)$. In order to obtain the free energy in the GL form we keep only the modes with $\vec{k}$ close to $\vec{Q}$[32]. For sake of simplicity we shift the wave vectors of the Brillouin zone by $\vec{Q}$ and therefore we consider only the modes close to $\vec{k}=0$ ($k<\Lambda$). For small $\vec{k}$ values, the Fourier transform of the coupling constant $J^{\psi(M)}(k)$ can be approximated as

$$J^{\psi(M)}(k) = J - \frac{1}{2}Jk^2 + O(k)^4 \tag{B2}$$

where we scaled J as J/z, z being the coordination number. After writing the free energy in terms of $\psi(\vec{k})$ and $M(\vec{k})$ and keeping only the modes with $k<\Lambda$, we go back to a real-space representation using the transformation

$$\phi_1(\vec{r}) = \frac{1}{\sqrt{V}}\sum_{k<\Lambda}e^{-i\vec{k}\cdot\vec{r}}\psi(\vec{k}) \tag{B3}$$

$$\phi_2(\vec{r}) = \frac{1}{\sqrt{V}}\sum_{k<\Lambda}e^{-i\vec{k}\cdot\vec{r}}M(\vec{k})\,. \tag{B4}$$

Indeed in Eqs. (B3) and (B4) the sum is on a discrete non-periodic set of wave vectors $\vec{k}$ with $k<\Lambda$, therefore the fields $\phi_1(\vec{r})$ and $\phi_2(\vec{r})$ are slowly varying and continuous. In terms of the fields $\phi_1(\vec{r})$ and $\phi_2(\vec{r})$ the free GL energy becomes

$$\begin{aligned} F = &\int \mathrm{d}\vec{r}\sum_{\alpha=1,2}\left(\frac{1}{2}\mu_\alpha(T)\Big(\phi_\alpha(\vec{r})\Big)^2+\frac{1}{2}k_1\left|\vec{\nabla}\phi_\alpha(\vec{r})\right|^2\right)\\ &+\tfrac{1}{4}\ u\sum_{\alpha,\beta=1,2}\Big(\phi_\alpha(\vec{r})\Big)^2\Big(\phi_\beta(\vec{r})\Big)^2\\ &-\tfrac{1}{4}\ k_2\sum_{\alpha,\beta=1,2}\left|\vec{\nabla}\phi_\alpha(\vec{r})\right|^2\left(\phi_\beta(\vec{r})\right)^2\\ &-\tfrac{1}{2}\ k_2\sum_{\alpha,\beta=1,2}\sum_{ij}\delta_{ij}\left(\partial_i\phi_\alpha(\vec{r})\right)\left(\partial_j\phi_\beta(\vec{r})\right)\phi_\alpha(\vec{r})\phi_\beta(\vec{r})\,. \end{aligned}$$

The coefficients k_1 and u are definite positive. To obtain the traditional form of the free energy we restrict the temperature dependence to the coefficient $\mu(T)$ of the quadratic term. The coupling coefficients are the same for $\phi_1(\vec{r})$ and $\phi_2(\vec{r})$ since this GL free energy has been derived from a microscopic model where hidden order and magnetization are related to each other, however the form of the free energy is completely general, and for

the URu_2Si_2 system was first discussed in the work of Ref. 21. For a sufficiently repulsive quartic interaction, it captures the competition and interplay between the HO and AFM order: the field $\phi_2(\vec{r})$ can develop only if the hidden order field $\phi_1(\vec{r})$ is suppressed. The gradient coupling term $k_2(\phi_2(\vec{r}))^2|\vec{\nabla}\phi_1(\vec{r})|^2$ was introduced and discussed in detail in Ref. 18 to explain the non-monotonic behavior of the antiferromagnetic fraction in the NMR spectrum. When $k_2 < 0$ inhomogeneities in ϕ_1 can nucleate a parasitic second order parameter ϕ_2 near impurities even when $\mu_2 > 0$.

[1] T. T. M. Palstra, A. A. Menovsky, J. vandenBerg, A. J. Dirkmaat, P. H. Kes, G. J. Nieuwenhuys, and J. A. Mydosh, Phys. Rev. Lett. **55**, 2727 (1985).

[2] C. Broholm, J. K. Kjems, W. J. L. Buyers, P. T. Matthews, T. T. M. Palstra, A. A. Menovsky, and J. A. Mydosh, Phys. Rev. Lett **58**, 1467 (1987).

[3] D. E. MacLaughlin, D. W. Cooke, R. H. Heffner, R. L. Hutson, M. W. McElfresh, M. E. Schillaci, H. D. Rempp, J. L. Smith, J. O. Willis, E. Zirngiebl, C. Boekema, R. L. Lichti, and J. Oostens, Phys. Rev. B **37**, 3153 (1988).

[4] G. Luke, A. Keren, L. P. Le, Y. J. Uemura, W. D. Wu, *et al.*, Hyperfine Interact. **85**, 397 (1994).

[5] K. Matsuda, Y. Kohori, T. Kohara, K. Kuwahara, and H. Amitsuka, Phys. Rev. Lett **87**, 087203 (2001).

[6] P. G. Niklowitz, C. Pfleiderer, T. Keller, M. Vojta, Y. K. Huang, and J. A. Mydosh, Phys. Rev. Lett. **104**, 106406 (2010).

[7] M. Yokoyama, H. Amitsuka, K. Tenya, K. Watanabe, S. Kawarazaki, H. Yoshizawa, and J. A. Mydosh, Phys. Rev. B **72**, 214419 (2005).

[8] A. Villaume, F. Bourdarot, E. Hassinger, S. Raymond, V. Taufour, D. Aoki, and J. Flouquet, Phys. Rev. B **78**, 012504 (2008).

[9] E. Hassinger, G. Knebel, K. Izawa, P. Lejay, B. Salce, and J. Flouquet, Phys. Rev. B **77**, 115117 (2008).

[10] C. R. Wiebe, J. A. Janik, G. J. MacDougall, G. M. Luke, J. D. Garrett, H. D. Zhou, Y.-J.Jo, L. Balicas, Y. Qiu, J. R. D. Copley, Z. Yamani, and W. J. L. Buyers, Nat. Phys. **3**, 96 (2007).

[11] A. F. Santander-Syro, M. Klein, F. L. Boariu, A. Nuber, P. Lejay, and F. Reinert, Nat. Phys. **5**, 637 (2009).

[12] A. V. Balatsky, A. Chantis, H. P. Dahal, D. Parker, and J. X. Zhu, Phys. Rev. B **79**, 214413 (2009).

[13] P. Chandra and P. Coleman, Nature Physics **5**, 625 (2009).

[14] F. Cricchio, F. Bultmark, O. Granas, and L. Nordstrom, Phys. Rev. Lett **103**, 107202 (2009).

[15] K. Haule and G. Kotliar, Nature Physics **5**, 796 (2009).

[16] S. Elgazzar, J. Rusz, A. M. Amft, P. M. Oppeneer, and J. Mydosh, Nature Materials **8**, 337 (2009).

[17] C. M. Varma and L. Zhu, Phys. Rev. Lett. **96**, 036405 (2006).

[18] S.-H. Baek, M. J. Graf, A. V. Balatsky, E. D. Bauer, J. C. Cooley, J. L. Smith, and N. J. Curro, Phys. Rev. B **81**, 132404 (2010).

[19] K. Haule and G. Kotliar, EuroPhysics Letters **89**, 57006 (2010).

[20] C. Broholm, H. Lin, P. T. Matthews, T. E. Mason, W. J. L. Buyers, M. F. Collins, A. A. Menovsky, J. A. Mydosh, and J. K. Kjems, Phys. Rev. B **43**, 12809 (1991).

[21] N. Shah, P. Chandra, P. Coleman, and J. A. Mydosh, Phys. Rev. B **61**, 564 (2000).

[22] Notice that the coefficients J^{ψ} and J^{M} contribute both to the massive and gradient term in the continuum formulation. In fact in order to derive the continuous free energy, we substitute $J_{ij} = J(\vec{R})$ with the Fourier transform $J(\vec{k}) = \sum_{\vec{R}} e^{i\vec{k}\cdot\vec{R}} J(\vec{R})$ (see Appendix B). The zero order term of $J(\vec{k})$ contributes to the massive term, while the quadratic term in k to the gradient term.

[23] P. Wolfle, Y. Dubi, and A. V. Balatsky, Phys. Rev. Lett. **105**, 246401; (2010).

[24] Y. Dubi and A. V. Balatsky, Phys. Rev. Lett. **106**, 086401 (2011).

[25] P. Santini and G. Amoretti, Phys. Rev. Lett. **73**, 1027 (1994).

[26] F. Ohkawa and H. Shimizu, J. Phys. Cond. Matt. **11**, L519 (1999).

[27] H. Harima, K. Myake, and J. Flouquet, J. Phys. Soc. Japan **79**, 033705 (2010).

[28] V. P. Mineev and M. E. Zhitomirsky, Phys. Rev. B **72**, 014432 (2005).

[29] A. Kiss and P. Fazekas, Phys. Rev. B **71**, 054415 (2005).

[30] M. Yokoyama, H. Amitsuka, S. Itoh, I. Kawasaki, K. Tenya, and H. Yoshizawa, J. Phys. Soc. Japan **73**, 545 (2004).

[31] K. Matsuda, Y. Kohori, T. Kohara, K. Kuwahara, and H. Amitsuka, Phys. Rev. Lett. **87**, 087203 (2001).

[32] D. J. Amit, *Field Theory, the Renormalization Group, and Critical Phenomena* (World Scientific, 1984).